A ribozyme and a catalytic DNA with peroxidase activity: active sites versus cofactor-binding sites

Paola Travascio, Andrew J Bennet, Dennis Y Wang and Dipankar Sen

Background: An 18-nucleotide DNA oligomer, *PS2.M*, derived using an *in vitro* selection method was previously reported to bind hemin (Fe(III)-protoporphyrinIX) with submicromolar affinity. The DNA–hemin complex exhibited DNA-enhanced peroxidative activity. *PS2.M* is guanine-rich and requires potassium ions to fold to its active conformation, consistent with its forming a guanine-quaduplex. In investigating the specific catalytic features of *PS2.M* we tested the peroxidative properties of its RNA version (*rPS2.M*) as well as that of an unrelated DNA guanine-quadruplex, *OXY4*.

Results: The hemin-binding affinity of *rPS2.M* was found to be 30-fold weaker than that of *PS2.M*. The UV–visible spectra and kinetics of enzymatic peroxidation of the RNA–hemin complex, however, were nearly identical to those of its DNA counterpart. Both displayed peroxidase activity substantially greater than those of heme proteins such as catalase and Fe(III)-myoglobin. Kinetic analysis suggested that *PS2.M* and *rPS2.M* catalyzed the breakdown of the hemin–hydrogen peroxide covalent complex to products. The hemin complex of folded *OXY4* (which bound hemin as strongly as did *rPS2.M*) had a distinct absorption spectrum and only a minor peroxidase activity above the background level.

Conclusions: The results indicated that it is possible for RNA and DNA of the same sequence to fold to form comparable cofactor-binding sites, and to show comparable catalytic behavior. The results further suggest that only a subset of cofactor-binding sites formed within folded nucleic acids might be able to function as active sites, by providing the appropriate chemical environments for catalysis.

Address: Institute of Molecular Biology & Biochemistry and Department of Chemistry, Simon Fraser University, Burnaby, BC Canada, V5A 1S6.

Correspondence: Dipankar Sen
E-mail: sen@sfu.ca

Introduction

The discovery of catalytic RNA molecules (ribozymes) [1,2] engendered the hypothesis of an 'RNA world' for the origin of life [3–7], according to which modern life forms were preceded by RNA molecules capable of self-replication, as well as the catalysis of different metabolic reactions. The RNA world hypothesis has stimulated much research into the catalytic repertoire of RNA. Recent developments in *in vitro* selection (SELEX) methods have facilitated investigations into both the structural and functional possibilities of RNA and DNA [8–11]. SELEX is basically an iterative procedure for enriching and selecting out RNA and DNA molecules that have specific binding and/or catalytic properties from random-sequence libraries. Both SELEX and the wide availability of modified nucleosides usable in automated chemical synthesis have enabled the examination of the structural and/or catalytic contributions of individual functional groups within RNA and DNA.

A central question about RNA catalysis focuses on possible roles for the ribose 2′ hydroxyl groups — whether in aiding the formation of diverse folded structures, or as a useful catalytic functionality (for example a nucleophile) in an otherwise functionality-poor biological polymer. Structurally, the presence of 2′ hydroxyls in RNA (and their absence in DNA) leads these two biopolymers to form divergent double helical structures and also, probably, to nonidentical repertoires of secondary and tertiary structures. For these reasons it has been recognized that a purely deoxy-version of an RNA molecule capable of a certain function (and *vice versa*) will generally be incapable of that function. Indeed, numerous reports on the *in vitro* selection of DNA and RNA 'aptamers' for binding specific molecular targets have broadly supported this notion, and have shown that distinct DNA and RNA sequence 'solutions' are obtained for a given binding or catalytic 'problem' (reviewed in [12]).

We had previously reported that a SELEX-derived 18-nucleotide DNA oligomer, *PS2.M*, when folded, bound hemin (Fe(III)-protoporphyrin IX) with strong affinity (< 0.5 μM) [13]. This DNA–hemin complex showed a DNA-enhanced peroxidative activity such that the

Figure 1

Absorption and binding curves for aptamer–hemin complexes.
(a) Absorbance curves of hemin (0.5 µM) fully bound to oligomers:
PS2.M, blue; *rPS2.M,* red; *OXY4,* green; and uncomplexed
monomeric hemin in the presence of the control oligomer *BLD,* black.
(b) Binding isotherms of hemin (0.5 µM) to *PS2.M* and *rPS2.M.* Blue
circles, *PS2.M*; red diamonds, *rPS2.M.*

$v_{cat}/v_{backgrd}$ ratio measured under optimized solution conditions was > 250 ($v_{backgrd}$ refers to the peroxidative activity of disaggregated hemin in the presence of a control DNA oligomer, *BLD*). *PS2.M* was guanine-rich, and required potassium ions to fold to its active conformation, consistent with its folding to form a guanine-quadruplex higher-order structure. In extending our investigation into the catalytic mechanism of *PS2.M* we wished to test the

properties of the RNA version of the *PS2.M* sequence. The goal was twofold: firstly, to see if such an RNA version of *PS2.M* ('*rPS2.M*') formed a hemin-binding site comparable to that of *PS2.M*; and secondly, to establish whether such a putative RNA–hemin complex demonstrated an RNA-enhanced peroxidase activity. We wished to determine in particular whether the binding of hemin to a folded DNA or RNA structure (especially a guanine-quadruplex) would lead trivially to an acceleration of the peroxidative property of the bound hemin, or whether additional features were required in hemin-binding sites to support catalysis.

Results

Hemin-binding by *PS2.M* and *rPS2.M*

We had shown previously that folded *PS2.M* strongly bound hemin, with a dissociation constant of < 0.5 µM (the precise K_d value of this very tight binding could not be measured by absorbance because measurements were unreliable at hemin concentrations of less than < 0.5 µM) [13]. In this present study we wished to determine accurately the binding constant of hemin to *PS2.M* using the sensitive fluorescence-based methods. Competition titrations were carried out with varying molar mixtures of hemin and a fluorescent porphyrin, NMM, which was found to bind to *PS2.M* with an affinity of 23.0 ± 0.6 nM (see the Materials and methods section). These experiments (data not shown) indicated that hemin bound to *PS2.M* with an affinity of 27 ± 2 nM. Such strong binding was consistent with our previous observation that hemin was an efficient competitive inhibitor for the catalysis of porphyrin metallation by a related DNA molecule, *PS5.M*, which was derived by *in vitro* selection techniques specifically for recognizing and binding to NMM [14,15].

The possible interaction of the RNA oligonucleotide, *rPS2.M*, with hemin was also investigated by absorption spectroscopy. A change in the Soret absorption band in response to titration with *rPS2.M* indicated that folded *rPS2.M* did bind hemin. A significantly greater concentration of *rPS2.M* (~15 µM, compared with ~1 µM *PS2.M*) was required to saturate the binding of 0.5 µM hemin. The fully saturated spectra of *PS2.M*–hemin and *rPS2.M*–hemin (Figure 1a) were found to be almost indistinguishable. Significantly, no spectral change was observed when hemin was titrated by the control RNA and DNA oligomers, *LIN4* and *BLD*, respectively. A curious observation was made when hemin was titrated with a DNA oligomer of telomeric origin, *OXY4* (of which the folded structure has been shown by high-resolution nuclear magnetic resonance (NMR) to be a guanine-quadruplex [16]). This titration gave rise to a hyperchromicity of the hemin Soret band (Figure 1a), consistent with hemin being able to bind to the folded *OXY4*. Even at binding saturation, however, the Soret band of *OXY4*–hemin had a smaller hyperchromicity than was observed with either *PS2.M* or *rPS2.M* (Figure 1a).

Although *rPS2.M*–hemin and *PS2.M*–hemin had almost identical spectra, the calculated dissociation constants for the two complexes differed significantly (binding isotherms shown in Figure 1b): the K_d for *PS2.M*–hemin was 27 ± 2 nM (see above), whereas that for *rPS2.M*–hemin was 900 ± 200 nM (Table 1). By comparison, *OXY4*–hemin, with its distinct spectroscopic signature, dissociated with a K_d of 700 ± 100 nM (Table 1), approximately equal to that of *rPS2.M*. Scatchard analysis on the interaction of hemin with the oligomers indicated that for *rPS2.M*–hemin and *OXY4*–hemin the binding stoichiometry ('n') of hemin:RNA/DNA was 1:1 (see Table 1). Owing to the very strong binding interaction of *PS2.M* and hemin, the binding stoichiometry of this complex could not be determined using the Scatchard method [17].

### Peroxidase activity of the different RNA–hemin and DNA–hemin complexes

The DNA-enhanced peroxidase activity of the *PS2.M*–hemin complex has been reported in 40KT buffer [13]. Under these conditions, peroxidation by *PS2.M*–hemin showed Michaelis–Menten-like kinetics as a function of concentration (as did uncomplexed, monomeric hemin, in the presence of the non-binding DNA oligomer *BLD*). The *PS2.M*–hemin complex and uncomplexed hemin had similar apparent K_d values for H_2O_2-binding (~3 mM), whereas the *PS2.M*–hemin complex had a higher k_{cat} than hemin alone. Under more optimal solution conditions, such as in buffer A (25 mM HEPES-NH_4OH, pH 8.0; 20 mM KCl, 200 mM NaCl, 1% v/v DMSO; 0.05% w/v Triton X-100), V_{obs}(*PS2.M*–hemin)/V_{obs}(hemin) was measured to be ~250 at low H_2O_2 concentrations. Yet it remained to be seen if saturation behavior was followed at high concentrations.

We re-examined the peroxidative behavior of *PS2.M*–hemin, and tested the *rPS2.M*–hemin complex for possible peroxidative activity (relative to that of hemin in the presence of the control RNA oligomer *LIN4*). The peroxidative behavior of both *PS2.M*–hemin and *rPS2.M*–hemin were checked both in 40KT buffer, and in the more optimal 20KH buffer (see the Materials and methods section). Figure 2a shows that when measured in 40KT buffer, both the background (uncomplexed hemin) and DNA-catalyzed peroxidation reactions had saturation

kinetics as functions of H_2O_2 concentration (up to concentrations of 6 mM). In contrast, the RNA-catalyzed peroxidation displayed a linear kinetic behavior up to a H_2O_2 concentration of 12 mM. To determine whether saturation could be reached at even higher H_2O_2 concentrations, the now very fast reaction rates were measured by stopped-flow methods. Even at H_2O_2 concentrations as high as 440 mM, no significant saturation of the rate was observed (a slight departure from linearity of the rate versus H_2O_2 concentration plot probably reflected the destruction of the active enzyme at very high H_2O_2 concentrations).

Interestingly, when peroxidations by *PS2.M*–hemin and *rPS2.M*–hemin were examined in the more optimal 20KH buffer, both complexes showed a nonsaturating, linear, kinetic behavior (Figure 2b). The measured second-order rate constants for *PS2.M*–hemin and *rPS2.M*–hemin under these conditions were almost identical — 1.02×10^4 M^{-1} s^{-1} and 1.00×10^4 M^{-1} s^{-1}, respectively (Table 2) — whereas the 'background' rate

Figure 2
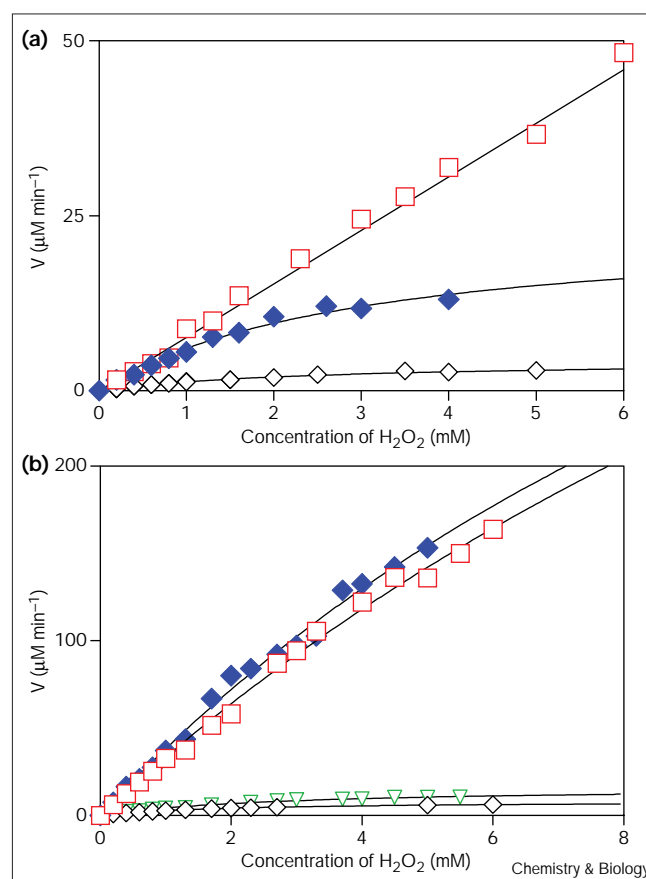
Plots of the initial rates of peroxidation as functions of hydrogen peroxide concentration in **(a)** 40KT buffer and in **(b)** 20KH buffer. Blue diamonds, *PS2.M*; red squares, *rPS2.M*; green inverted triangles, *OXY4*; black diamonds, uncomplexed hemin in the presence of oligomer controls..

Table 1

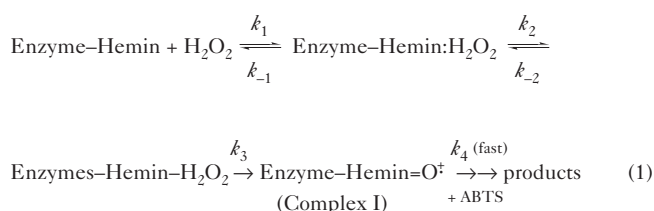Comparison of binding parameters of oligomer–hemin complexes.

Oligomer	K_d (µM)	n
PS2.M	0.027 ± 0.002	–
rPS2.M	0.9 ± 0.2	1.14 ± 0.056
OXY4	0.7 ± 0.01	1.006 ± 0.049

n is the binding stoichiometry.

constant for peroxidation by uncomplexed heme, measured in this buffer, was 1.40×10^2 M^{-1} s^{-1}. Thus, the *PS2.M*–hemin and *rPS2.M*–hemin complexes were approximately two orders of magnitude more reactive than the control.

The failure to observe saturation kinetics for enzymes is not an uncommon phenomenon. For example, both catalase and superoxide dismutase [18], and various hemin-based peroxidase model systems [19–21] show this kinetic behavior, although not necessarily for the same reasons. Equation 1 shows a reaction scheme for a typical peroxidase enzyme.

$$\text{Enzyme–Hemin} + H_2O_2 \underset{k_{-1}}{\overset{k_1}{\rightleftharpoons}} \text{Enzyme–Hemin:}H_2O_2 \underset{k_{-2}}{\overset{k_2}{\rightleftharpoons}}$$

$$\text{Enzymes–Hemin–}H_2O_2 \overset{k_3}{\rightarrow} \underset{(\text{Complex I})}{\text{Enzyme–Hemin=}O^\ddagger} \overset{k_4 \text{ (fast)}}{\underset{+ \text{ ABTS}}{\rightarrow\rightarrow}} \text{products} \qquad (1)$$

In the cases of fast (diffusion-limited) enzymes such as catalase, k_1 is the rate-determining step, with $k_2 > k_{-1}$. In our experiments, however, the observation of 'saturation' kinetics more probably indicated the formation, possibly reversibly, of a covalent iron–peroxide complex (Enzyme–Hemin–H_2O_2, see equation 1) rather than the formation of a non-covalent Michaelis complex. Consistent with this argument is the observation that uncomplexed hemin (in both the 40KT and 20KH buffers) and the *PS2.M*–hemin complex (in the 40KT buffer) showed saturation behavior (i.e. at high H_2O_2 concentration, k_3 is probably the rate-determining step). In contrast, in 20KH buffer, such behavior was not observed for either *PS2.M*–hemin or *rPS2.M*–hemin. The simplest explanation for this observation is that the DNA and RNA components of the *PS2.M*–hemin and *rPS.2M*–hemin complexes catalyze the breakdown of the hemin–H_2O_2 covalent complex towards products, such that its formation (defined by k_2) is rate-determining. The rate law for such an enzyme is best described by: V = k_2' [H_2O_2][*rPS2.M*–hemin], where $k_2' = k_1k_2/k_{-1}$ (equation 1). A value of $k_2' = 1.30 \times 10^3$ M^{-1} s^{-1} for the *rPS2.M*–hemin complex was derived from a linear plot of rate versus enzyme concentration (in 40KT buffer, with H_2O_2 concentration held constant at 1 mM). The k_2' values measured for both *PS2.M* and *rPS2.M* in the optimal 20KH buffer were greater than their respective catalytic parameters measured in 40KT buffer (*PS2.M*: $k_{cat}/K_d = 1.34 \times 10^3$ M^{-1}s^{-1}; and for *rPS2.M*: $k_2' = 1.30 \times 10^3$ M^{-1}s^{-1}).

Interestingly, the DNA oligomer *OXY4*, which had been shown to bind hemin with an affinity comparable to that of *rPS2.M*, was not found to catalyze peroxidation significantly above that of uncomplexed hemin, when measured in 20KH buffer (see Table 2). From this result it can be concluded that the simple fact of hemin complexation by a folded DNA or RNA molecule is not sufficient to enhance the intrinsic peroxidative activity of uncomplexed, monomeric hemin. In other words, catalysis is not a trivial consequence of hemin binding to a folded DNA/RNA molecule (interestingly, it has been reported that *OXY4* does not catalyze the metallation of porphyrins either, whereas *PS2.M* and related DNA sequences [22] do).

As described above, Scatchard analysis [23] was used to demonstrate that *rPS2.M* and *OXY4* bound hemin in DNA/RNA:hemin ratios of ~1:1. We now used native gel electrophoresis in the presence of 20 mM potassium chloride to investigate whether the active conformations of *PS2.M* and *rPS2.M* were intramolecularly folded monomers, or whether they were dimers or higher intermolecular aggregates. The results (data not shown) indicated that in the absence as well as in the presence of hemin both *PS2.M* and *rPS2.M* migrated as folded monomers (with no trace of higher-order complexes visible). The folded monomer, however, migrated as two to three electrophoretically distinct but closely spaced conformers in the absence of hemin (although for the *PS2.M*–hemin complex only one major conformer was seen). Such folding polymorphisms under comparable electrophoretic conditions have also been reported for guanine-rich telomeric oligomers such as *OXY4* [24].

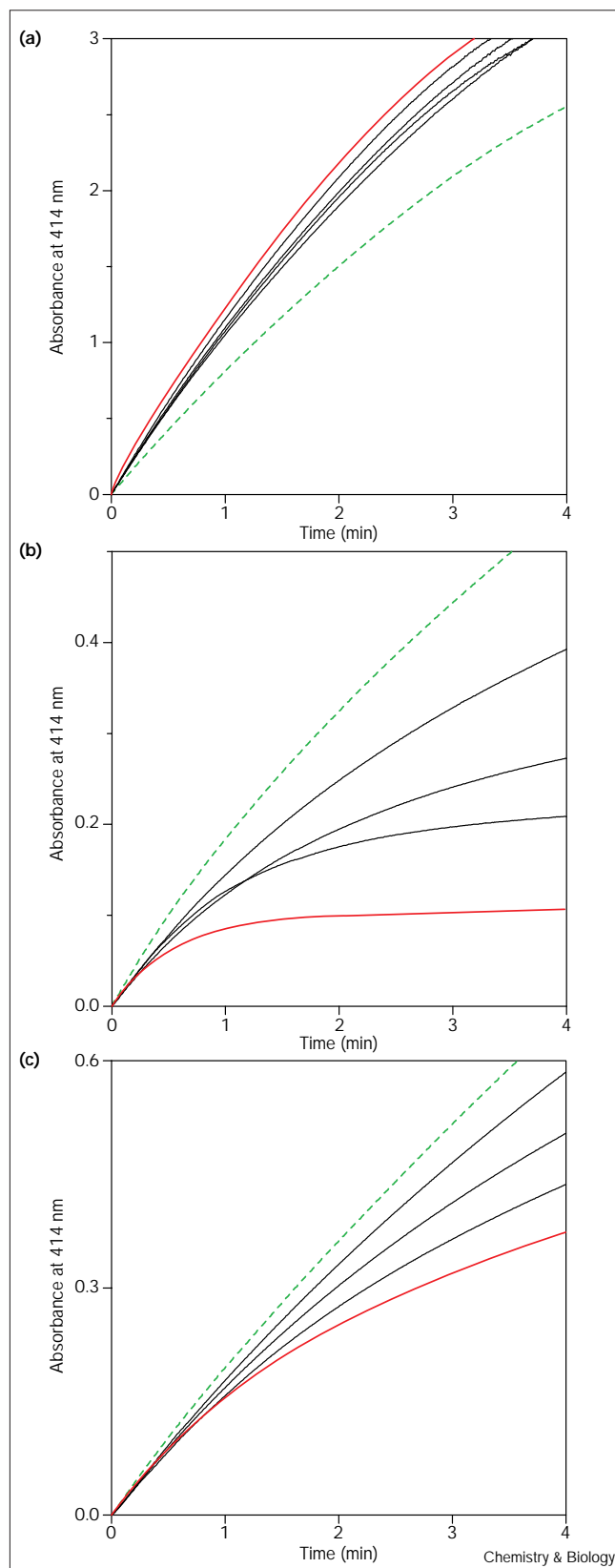### Protection of hemin from auto-oxidation
It is known that the active hemin moiety within oxidative heme-enzymes [25,26] as well as in many hemin-utilizing

Table 2

Comparison of kinetic parameters for peroxidation by hemin complexes.

Enzymes	k_{cat} (min^{-1})	K_M (mM)	k_{cat}/K_M (M^{-1}s^{-1})	k_2' (M^{-1}s^{-1})
Hemin*	26	3.0	1.4×10^2	NA
*PS2.M**	NA	NA	NA	1.02×10^4
*rPS2.M**	NA	NA	NA	1.00×10^4
OXY4 *	100	3.3	4.9×10^2	NA
HRP	1.98×10^4	0.033	$\sim 10^7$	NA
Catalase	NA	NA	NA	$\sim 10^2$–10^3
WT metMb[†]	NR	NR	5.4×10^2	NA
Mut metMb[†]	NR	NR	1.34×10^4	NA
Mut metMb[‡]	NR	NR	$< 10^2$	NA
Catalytic Ab[§]	NR	NR	2.33×10^2	NA

*As determined in the optimal 20KH buffer (see the Materials and methods section). [†]Data were obtained from reference [36]. Mut metMb is a T39I/K45D/F46L/I107L mutant of metMb (MetMb is ferrimyogobin or metmyoglobin). [‡]Mut metMb is a L29H/H64L mutant [35]. The mutants are defined using single letter amino acid code. [§]Catalytic antibody with peroxidase activity [55]. HRP, horseradish peroxidase; WT, wild type; NR, not reported; NA, not applicable.

Figure 3

Peroxidation rate versus time plots at different substrate (ABTS) concentrations. **(a)** *PS2.M*–hemin, **(b)** uncomplexed hemin and **(c)** *OXY4*–hemin. Concentrations of ABTS used were: 1.0, 8.0, 12.0, 16.0, 20.0 and 40.0 mM for *PS2.M*–hemin; 1.0, 5.0, 10.0, 20.0, 40.0 mM for hemin; and, 1.0, 5.0, 10.0, 20.0 and 50.0 mM for *OXY4*–hemin. Green line, highest concentration of ABTS. The red trace, showing data at the lowest concentration of ABTS, is composed of original data points, taken at 0.5 s time intervals. The black lines show all the concentrations in between.

To explore the character of hemin-binding sites within those folded nucleic acid complexes that significantly enhanced catalysis (such as *PS2.M*–hemin and *rPS2.M*–hemin) and those that did so poorly (such as *OXY4*–hemin), we investigated the degree to which these various complexes helped to protect the active hemin moiety from inactivation by auto-oxidation. The reactive 'lifetimes' of the different complexes were therefore examined as functions of the oxidative substrate ABTS (2,2'-azinobis(3-ethylbenzothiozoline)-6-sulfonic acid) concentration. Our earlier work with the *PS2.M*–hemin complex had indicated a zero-order dependence of *PS2.M*–hemin catalyzed rates on ABTS concentration [13]. Figure 3 shows rate versus time plots for different ABTS concentrations (with H_2O_2 concentration fixed at 4 mM) for peroxidation by uncomplexed hemin (Figure 3b), *PS2.M*–hemin (Figure 3a), and *OXY4*–hemin (Figure 3c) respectively. It can be seen that in all cases, for at least up to 20 mM ABTS, the initial rate (within the first 20–30 seconds following the commencement of the reaction) is independent of ABTS. Although the rate versus time dependence is stable for *PS2.M*–hemin (and for *rPS2.M*–hemin; data not shown) within reasonable ABTS concentrations, for uncomplexed hemin the reaction is progressively quenched (within 30–60 seconds) at all — but especially, low — ABTS concentrations. Here, increasing concentrations of ABTS appear to ameliorate this quenching, which is probably because of an auto-oxidative destruction of the hemin cofactor in the presence of H_2O_2 [27]. At low ABTS concentrations, the 'naked' hemin is rapidly oxidized and deactivated; however, higher concentrations of the oxidizable substrate ABTS afford increasing degrees of protection to the hemin. By contrast, the stability of the reaction curves for the *PS2.M*–hemin and *rPS2.M*–hemin complexes indicate that the hemin moieties in these complexes are effectively protected from inactivation by their nucleic acid environments.

By comparison to the above, *OXY4*–hemin (Figure 3c) appears to offer only a modest protection against inactivation, unlike *rPS2.M* (which binds hemin with an affinity comparable to that of *OXY4*) and *PS2.M*. The above data, together with the UV–visible spectra, suggest that the immediate microenvironment 'experienced' by the hemin

model compounds [21] are offered a substantial protection against auto-oxidation in the presence of H_2O_2.

moiety to be structurally different between the *OXY4* and the *PS2.M*/*rPS2.M* systems. Alternatively, the positioning of the hemin in these systems might be dissimilar.

Discussion

How effective are *PS2.M*–hemin and *rPS2.M*–hemin as enzymes?

Table 2 shows that the apparent second-order rate constants for peroxidation by both *PS2.M*–hemin and *rPS2.M*–hemin are ~1.0×10^4 $M^{-1}s^{-1}$. Although this is a modest number compared with the k_{cat}/K_M value (0.9×10^7 $M^{-1}s^{-1}$) of an evolved and diffusion-limited enzyme such as horseradish peroxidase [28] it should be remembered that our catalysts were not 'evolved' to include a peroxide-binding site. Regardless, the efficiency of peroxidation by *PS2.M*–hemin and *rPS2.M*–hemin is superior to those of a number of other Fe(III)-hemoproteins. For instance, catalases are known to have peroxidase activity, albeit with efficiencies (k ~10^2–10^3 $M^{-1}s^{-1}$) lower than for their major catalytic activity of H_2O_2 degradation [29,30]. Yet other heme proteins, including ferrimyoglobin (metmyoglobin or metMb) [31–33] and ferrihemoglobin (methemoglobin or metHb) [34] are able to utilize H_2O_2 to oxidize a wide range of substrates, but with efficiencies poorer (k_{cat}/K_M values of ~10^2 $M^{-1}s^{-1}$) than *PS2.M*–hemin or *rPS2.M*–hemin (Table 2). In recent studies, both site-directed mutagenesis [35] and *in vitro* evolution of myoglobin [36] have been attempted to enhance the peroxidase activity of metMb (Table 2). Comparison of the catalytic efficiency of *PS2.M*–hemin and *rPS2.M*–hemin with these mutagenized heme-proteins (some of which were studied under solution conditions similar to the 40KT buffer reported in this paper [18,36]), indicates, again, that the *PS2.M*–hemin and *rPS2.M*–hemin have efficiencies similar to or higher than those of the 'improved' metMb proteins.

Similarities and differences between *PS2.M*–hemin and *rPS2.M*–hemin

It is curious that whereas the RNA oligomer *rPS2.M* binds hemin significantly more weakly than does its DNA counterpart, the final chemical environments provided by the two folded oligomers appear to be remarkably similar, as indicated by both the spectral and catalytic data. The tighter binding of hemin by *PS2.M* might have two quite distinct causes: firstly, the high affinity of *PS2.M* for hemin might simply reflect the fact that the original *in vitro* selection for hemin-binding was carried out from a random sequence DNA (and not RNA) library [14]. Whether this is the cause for the observed difference in hemin-affinity between *PS2.M* and *rPS2.M* could be investigated by testing a DNA version of an RNA aptamer selected for hemin binding. As such, an RNA aptamer (a guanine-rich 19-mer) reported for the binding of amino-methylmesoporphyrin IX (a porphyrin that shares a number of structural features with hemin) might prove suitable for this purpose [37]. Second, an alternative explanation might be

that DNA intrinsically folds to form better binding sites for hemin. The absence and presence, respectively, of 2′ hydroxyl groups in the backbones of DNA and RNA probably impart different rigidities to the folded structures of *PS2.M* and *rPS2.M*, comparably to what is known about the relative rigidities of DNA ('B'-type) and RNA ('A'-type) double helices. Both *PS2.M* and *rPS2.M* appear to fold to guanine-quadruplex structures. In the case of *PS2.M*, this is indicated by the absolute requirement for potassium ion for its hemin-binding property (guanine-quadruplexes have been shown to be maximally stabilized by the potassium ion [38,39]). The *rPS2.M* is by analogy probably a guanine-quadruplex as well, as indicated by the similarities in its hemin-binding and spectroscopic properties to those of *PS2.M*. The folded structure of *rPS2.M*, however, might be more stable than that of *PS2.M*, given an observed insensitivity of the hemin-binding ability of *rPS2.M* to potassium (data not shown). A comparable result has been reported for guanine-quadruplex-forming DNA and RNA aptamers for riboflavin binding [23]. Recently, a large number of papers have reported high resolution structural data on DNA guanine-quadruplexes [39]; however, data on RNA quadruplexes are rare. An NMR study of an RNA quadruplex reported the predominance of the C3′-endo sugar pucker [40]; whereas DNA guanine-quadruplexes contain mostly the C2′-endo sugar pucker [16,41–43]. These sugar-pucker preferences in quadruplexes mirror those found in duplex DNA and RNA, and might in turn be related to a greater conformational flexibility [44,45] of DNA quadruplexes relative to their RNA counterparts. Such flexibility might in turn correlate with a superior ability of DNA to bind ligands such as hemin [46]. Whether this is indeed the root cause for the significantly better binding of hemin by *PS2.M* is being actively investigated in our laboratory.

What is the nature of the active sites within *PS2.M*, *rPS2.M* and the hemin-binding site in *OXY4*?

It is undoubtedly possible, in a complicated folded structure such as a DNA or RNA quadruplex, to have multiple kinds of binding sites for a ligand such as hemin. In addition to the possibility of intercalating between adjacent quartets, hemin could interact with additional structural features of quadruplexes, including the connecting loops, the flat outer faces of the two terminal guanine-quartets, as well as with the four nonidentical grooves. It is crucial in this respect that *PS2.M* and *rPS2.M* on the one hand, and *OXY4* on the other, present nonidentical binding sites to hemin. Such a conclusion can be arrived at from the cumulative evidence of spectral fingerprints, catalytic ability, and differential protection afforded the bound hemin moiety. In the cases of *PS2.M* and *rPS2.M*, we have shown that although there is a significant difference in their binding affinity for hemin, once hemin is bound to either oligomer it displays the same enhanced catalytic performance. This indicates that the chemical

microenvironments provided hemin within the binding sites of *PS2.M* and *rPS2.M* are very similar.

The data presented above do not provide a direct picture of the different binding modes and of the active sites. It might be the case with *OXY4* (d5′-T$_4$G$_4$T$_4$G$_4$T$_4$G$_4$T$_4$G$_4$-3′), which folds to form four compactly stacked guanine-quartets (a high resolution NMR structure has been reported for a closely related molecule, *OXY3.5*, which lacks the four 5′ terminal thymines [16]), that hemin might bind by stacking upon a terminal quartet. Such a mode of binding to a quadruplex by the DNA ligand PIPER (*N*,*N*′-bis[2-1(-piperidino)-ethyl]-3-,4,9,10-pery-lene-tetracarboxylic diimide) has been demonstrated using high-resolution NMR [47]. For a structure such as folded *OXY4*, there is probably a high energy cost associated with separating adjacent quartets and unwinding the quadruplex in order to intercalate a ligand. In fact, intercalation of bulky ligands such as porphyrins into quadruplexes containing standard guanine-quartets has been considered unlikely [48]. In contrast, *PS2.M* (d5′*GTGGG*TA*GGGCGGG*TT*GG*-3′) and *rPS2.M*, with their twelve guanine bases (italicized), appear to form a strained guanine-quadruplex (Y. Li and D.S., unpublished observations), containing very short loops of either one or two nucleotides (whereas *OXY4* has generous loops of four thymine bases each). Of the three putative quartets in *PS2.M* and *rPS2.M*, moreover, the one that incorporates the isolated 5′ terminal guanine might be intrinsically 'looser' or less stable. Strained, or 'looser', quadruplexes formed by *PS2.M* and *rPS2.M* might permit a partial intercalation of hemin between quartets, a model that would be consistent with the high observed spectral hyperchromicity and also the greater protection afforded their bound hemins by these two catalytic oligomers. An 'outside-stacked' mode of hemin-binding by *OXY4* could, by contrast, give rise to a lesser hyperchromicity, and also to only a partial protection of the bound heme from inactivation.

Although at this stage we do not have a detailed picture of the hemin-binding active sites of *PS2.M* and *rPS2.M*, their kinetic behavior provides a clue to their catalytic mechanism. We propose that in *PS2.M* and *rPS2.M*, the hemin-bound Michaelis complex (enzymes–hemin Equation 1) activates the iron for reaction with H$_2$O$_2$ and furthermore, that the breakdown of the covalent iron–peroxide complex to products is accelerated, perhaps by specific interactions within the active sites of *PS2.M* and *rPS2.M*. We are actively investigating the mechanism, as well as the nature, of the active species involved in the DNA/RNA catalysis of peroxidation. Future experiments will also focus on elucidating the mode of hemin binding to catalytic as opposed to noncatalytic DNA and RNA systems, particularly with respect to the importance of positioning of specific nucleic acid functionalities with respect to the hemin moiety.

Finally, the discovery of an RNA–hemin complex with enhanced peroxidase activity relative to hemin itself is of interest to the 'RNA world' hypothesis. Reduction–oxidation (redox) reactions comprise nearly one quarter of the total number of classified enzymatic reactions in modern primary metabolism [7]. It is conceivable that in an 'RNA world', ribozymes catalyzing metabolically important redox reactions might have recruited hemin or hemin-like molecules as cofactors.

Significance

In this paper we report a small RNA molecule, *rPS2.M*, that binds hemin and exhibits a peroxidase activity superior to that of some Fe(III)-hemoproteins. This work also provides evidence that in certain instances RNA and DNA of the same nucleotide sequence are able to form comparable cofactor-binding sites, and that only a subset of such sites are 'active sites', capable of promoting catalysis. Nucleic-acid-enhanced catalysis of hemin-dependent reactions is therefore not a trivial consequence of the binding of hemin by a folded DNA or RNA molecule. In this instance, moreover, we have provided experimental evidence that the mechanism of both *rPS2.M* and its DNA equivalent, *PS2.M*, probably incorporates the nucleic-acid-catalyzed breakdown of the hemin–H$_2$O$_2$ covalent complex to products.

Nearly one quarter of all classified enzymatic reactions are oxidation–reduction (redox) reactions. It is possible that in an RNA world, ribozymes that catalyzed such metabolically important reactions might have sequestered hemin-like molecules as cofactors.

Materials and methods
Porphyrins
Hemin and *N*-methylmesoporphyrin IX (NMM) were purchased from Porphyrin Products,(Logan, Utah), and used without further purification. Their concentrations were determined using standard spectroscopic methods [49,50]. Porphyrin stock solutions (5 mM or 8 mM) were prepared in DMSO (1 ml). Diluted stock solutions (25 µM or 100 µM) were made up in DMSO and frozen and stored in the dark at −20°C. These solutions were found to be stable for up to one month. All chemicals used were of reagent grade. All buffers (that is 40KT and 20KH – see below) used for spectroscopic and/or peroxidation measurements contained the nonionic detergent Triton X-100 (0.05% w/v). This low concentration of detergent was found to be optimal for the disaggregation of hemin, as well as for its optimal peroxidative activity [13].

RNA and DNA oligonucleotides
DNA and RNA oligomers were synthesized at the University Core DNA Services (University of Calgary). They were purified in preparative polyacrylamide gels and stored in TE buffer (10 mM Tris, pH 7.5, 0.1 mM EDTA) at −20°C. The nucleotide sequences of the oligomers are given below:

PS2.M: d5′-GTGG GTAG GGCG GGTT GG-3′

rPS2.M: r5′-GUGG GUAG GGCG GGUU GG-3′

OXY4: d5′-TTTT GGGG TTTT GGGG TTTT GGGG TTTT GGGG-3′

BLD: d5′-AATA GGAC TCAC TATA GGAA GAGA TGG-3′

LIN4: r5′-UUCC CUGA GACC UCAA GUGU GA-3′

Absorbance spectroscopy of RNA–hemin and DNA–hemin complexes

Stock solutions of oligomers were heated to 95°C in TE buffer, and allowed to cool to room temperature. Different concentrations of oligomers (0–50 μM) were made up to 40KT buffer (50 mM MES, 100 mM Tris-acetate, pH 6.2, 40 mM KOAc, 0.05% Triton X-100, 1% DMSO) to allow proper folding. Each solution was then made up to 0.5 μM hemin (final), incubated for 30 min, and their UV–visible spectra were recorded. Dissociation constants, K_d, were determined by fitting the spectroscopic data to the following equation [51]: $[DNA_o] = K_d(A–A_o)/(A\infty–A) + [P_o](A–A_o)/(A\infty–A_o)$, in which A∞ describes hemin absorbances of the Soret band (404–407 nm) at RNA/DNA concentrations where hemin-binding is saturated; A_o describes absorbance at 398 nm in the absence of DNA/RNA aptamers; DNA_o, the concentration of oligomer; and P_o, the fixed concentration of hemin.

Fluorescence determination of the dissociation constant for PS2.M–hemin

Fluorescence measurements were made in a Photon Technology International (PTI) Spectrofluorimeter. Emission spectra for NMM were obtained with excitation wavelength set at 397 nm, with a 3 nm slit width. Emission spectra were recorded between 550 and 700 nm, at ambient temperature (23°C). Hemin itself does not fluoresce; therefore, its K_d was determined indirectly, via competition [52] for binding to *PS2.M* with the fluorescent porphyrin, *N*-methylmesoporphyrin (NMM). First, the K_d for NMM was determined fluorimetrically in 40KT buffer, giving a value of 23.0 ± 0.6 nM. Then, the displacement of NMM by hemin was followed fluorimetrically, by monitoring the decrease in NMM fluorescence at 608 nm. The data were fit to a sigmoidal competitive-binding curve (Program Prism™ 2.0) with the expression, $F = F_{max} + (F_{max}–F_{min})/(1 + 10^{X-log\ EC_{50}})$ [53], where X is log [competitor], F the measured fluorescence, F_{max} and F_{min}, respectively, the fluorescence intensities in the complete absence of and in the presence of saturating concentrations of the competitor (the upper and lower plateaux of the sigmoidal curve), and EC_{50} is the concentration of competitor required to displace half of the specifically bound NMM. The dissociation constant (K_i) for the competitor, hemin, was calculated by using the following equation [54], $K_i = EC50/(1 + [ligand]/K_d)$, where K_d is the dissociation constant for the ligand NMM (as determined under equivalent experimental conditions).

Kinetic measurements of peroxidase reactions

Rates of ABTS oxidation by uncomplexed hemin and by the DNA/RNA–hemin complexes were monitored by measuring the appearance of the ABTS radical cation (ABTS•⁺) at 414 nm using either a Cary-3E UV–Vis spectrophotometer equipped with the Cary six-cell Peltier constant temperature accessory or an Applied Photophysics SX-18MV stopped-flow apparatus thermostatted with a Lauda RM6 circulating water bath, at 20°C. Slower reactions were initiated by injection of a stock solution of H_2O_2 (0.44 M) into an equilibrated mixture of ABTS plus uncomplexed hemin or hemin in the presence of RNA/DNA oligomers in 40KT buffer (see above) or in 20KH buffer (50 mM HEPES–NH₄OH, pH 8.0, 20 mM KCl, 0.05% Triton X-100, 1% DMSO). Whereas for the stopped-flow reactions equal volumes of a 2× solution of H_2O_2 were mixed with a 2× solution of ABTS and the *rPS2.M*–hemin complex. Initial rates were calculated by performing a linear fit of the absorbance versus time data. Most experiments were repeated, and agreement was found in each case within ± 10%.

Electrophoretic analysis of oligonucleotides and hemin–oligonucleotide complexes

5′ end-labeled oligonucleotides (0.9–1.4 mM) were denatured at 90°–95°C in TE buffer and then cooled to room temperature. The oligomers were made up to their final salt concentrations of 50 mM HEPES-Tris, pH 7.8, 20 mM KCl, and 0.25% Triton X-100, and allowed to fold for 30 min. Hemin, where appropriate, was added to final concentrations of 100 μM and allowed to complex with the oligomers for 30 min. The samples were loaded in 16% nondenaturing polyacrylamide gels in 50 mM TBE buffer, pH 8.0, supplemented with 20 mM of either LiCl or KCl. Gels were run at room temperature (~23°C) and autoradiographed at 4°C without drying.

References
1. Kruger, K., Grabowski, P.J., Zaug, A.J., Sauds, J., Gottschling, D.E. & Cech, T.R. (1982). Self-splicing RNA: autoexcision and autocyclization of the ribosomal RNA intervening sequence of Tetrahymena. *Cell* **31**, 147-157.
2. Guerrier-Takada, C., Gardiner, K., Marsh, T., Pace, N. & Altman, S. (1983). The RNA moiety of ribonuclease P is the catalytic subunit of the enzyme. *Cell* **35**, 849-857.
3. Gilbert, W. (1986). The RNA World. *Nature* **319**, 618.
4. Benner, S.A., Ellington, A.D. & Traver, A. (1989). Modern metabolism as a palimpest of the RNA world. *Proc. Natl Acad. Sci. USA* **86**, 7054-7058.
5. Lewin, R. (1986). RNA catalysis gives fresh prospective on the origin of life. *Science* **231**, 545-546.
6. Joyce, G.F. (1989). RNA evolution and the origins of life. *Nature* **338**, 217-224.
7. White, H.B. (1982). *Pyridine Nucleotide Coenzymes.* Academic Press, Inc., New York.
8. Ellington, A.D. & Szostak, J.W. (1990). *In vitro* selection of RNA molecule that bind specific ligands. *Nature* **346**, 818-822.
9. Joyce, G.F. (1994). *In vitro* evolution of nucleic acids. *Curr. Opin. Struct. Biol.* **4**, 331-336.
10. Breaker, R.R. (1997). *In vitro* selection of catalytic polynucleotides. *Chem. Rev.* **97**, 371-390.
11. Tuerk, L. & Gold, L. (1990). Systematic evolution of ligands by exponential enrichment: RNA ligands to bacteriophage T4 DNA polymerase. *Science* **249**, 505.
12. Sen, D. (1999). DNA selection and amplification. In *Comprehensive Natural Products Chemistry*, eds. Barton, D. & Nakanishi, K. (Elsevier, Oxford), Vol. 7, pp. 615-640.
13. Travascio, P., Li, Y. & Sen, D. (1998). DNA-enhanced peroxidase activity of a DNA aptamer–hemin complex. *Chem. Biol.* **5**, 505-517.
14. Li, Y., Geyer, R. & Sen, D. (1996). Recognition of anionic porphyrins by DNA aptamers. *Biochemistry* **35**, 6911-6922.
15. Li, Y. & Sen, D. (1997). A catalytic DNA for porphyrin metallation. *Nat. Struct. Biol.* **3**, 743-747.
16. Smith, F.W. & Feigon, J. (1992). Quadruplex structure of *Oxytricha* telomeric DNA oligonucleotides. *Nature* **356**, 164-168.
17. van Holde, K.E. (1985). *Physical Biochemistry.* Prentice-Hall, Inc., Englewood Cliffs, New Jersey.
18. Putter, J. & Becker, R. (1983). Enzymes 1: oxidoreductases, Transferases. In *Methods of Enzymology Analysis.* (Bergmeyer, H. U., Bergmeyer, J. & Grassl, M., eds.), Vol. 3, pp. 273-286, Verlag Chemie, Basel.
19. Almarsson, O. & Bruice, T.C. (1995). A homolytic mechanism of O–O bond scission prevails in the reactions of alkylhydroperoxides with an octacationic tetraphenylporphinato-iron(III) complex in aqueous solution. *J. Am. Chem. Soc.* **117**, 4533-4544.
20. Zipplies, M.F., Lee, W.A. & Bruice, T.C. (1986). Influence of hydrogen ion activity and general acid–base catalyis on the rate of decomposition of hydrogen peroxide by a novel nonaggregating water-soluble iron(III) tetraphenylporphyrin derivative. *J. Am. Chem. Soc.* **108**, 4433-4445.
21. Traylor, T.G., Lee, W.A. & Stynes, D.V. (1984). Model compound studies related to peroxidases, mechanism of reactions of hemins with peracids. *J. Am. Chem. Soc.* **106**, 755-764.
22. Li, Y. & Sen, D. (1997). Towards an efficient DNAzyme. *Biochemistry* **36**, 5589-5599.
23. Lauhon, C.T. & Szostak, J.W. (1995). RNA aptamers that bind flavin and nicotinamide redox cofactors. *J. Am. Chem. Soc.* **117**, 1246-1257.

24. Williamson, J.R., Raghuraman, M.K. & Cech, T.R. (1989). Monovalent cation-induced structure of telomeric DNA: the G-quartet model. *Cell* **59**, 871-880.

25. Brown, S.B., Jones, P. & Suggett, A. (1968). Reactions between hemin and hydrogen peroxide. *J. Chem. Soc. Faraday Trans.* **64**, 986-993.

26. Jones, P., Prudhoe, K. & Robson, T. (1973). Oxidation of deuteroferrihaem by hydrogen peroxide. *Biochem. J.* **35**, 361-365.

27. Brown, S.B. & Jones, P. (1968). Reactions between heamin and hydrogen peroxide: destructive oxidation of heamin. *J. Chem. Soc. Faraday Trans.* **64**, 994-1005.

28. Dunford, H.B. & Stillman, J.S. (1976). On the function and mechanism of action of peroxidases. *Coord. Chem. Rev.* **19**, 187-251.

29. Chance, B. & Huennekens, F.M. (1963). Investigation of rates and mechanism of reactions. In *Techniques of Organic Chemistry.* (Weissberger, A., ed.), Vol. III, Interscience Publisher, New York.

30. Tauber, H. (1953). Oxidation of pyrogallol to puppurogallin by crystalline catalase. *J. Biol. Chem.* **205**, 395-401.

31. George, P. & Irvine, D.H. (1952). The reaction between metmyoglobin and hydrogen peroxide. *Biochem. J.* **52**, 511-517.

32. Keilin, D. & Hartrel, E.E. (1955). Catalase, Peroxidase and metmyoglobin as catalysts of coupled peroxidatic reactions. *Biochem. J.* **60**, 310-325.

33. King, N.K. & Winfield, M.E. (1963). The mechanism of metmyoglobin oxidation. *J. Biol. Chem.* **238**, 1520-1528.

34. Shiga, T. & Imaizumi, K. (1975). Electron spin resonance study on peroxidase and oxidase reactions HRP and methemoglobin. *Arch. Biochem. Biophys.* **167**, 469-479.

35. Ozaki, S., Matsui, T. & Watanabe, Y. (1997). Conversion of myoglobin into a peroxyganase: a catalytic intermediate of sulfoxidation and epoxidation by the F43H/H64L mutant. *J. Am. Chem. Soc.* **119**, 6666-6667.

36. Wan, L., Twitchett, M.B., Eltis, L.D., Mauk, A.G. & Smith, M. (1998). *In vitro* evolution of horse heart myoglobin to increase peroxidase activity. *Proc. Natl Acad. Sci. USA* **95**, 12825-12831.

37. Conn, M.M., Prudent, J.R. & Schultz, P.G. (1996). Porphyrin metallation catalyzed by a small RNA molecule. *J. Am. Chem. Soc.* **118**, 7012-7013.

38. Williamson, J.R. (1994). G-quartet structures in telomeric DNA. *Ann. Rev. Biophys. Biomol. Struct.* **23**, 703-730.

39. Wellinger, R.J. & Sen, D. (1997). The DNA structures at the ends of eukaryotic chromosomes. *Eur. J. Cancer* **33**, 735-749.

40. Cheong, C. & Moore, P.B. (1992). Solution structure of an unusually stable RNA tetraplex containing G- and U-quartet structures. *Biochemistry* **31**, 8406-8414.

41. Laughlan, G., *et al.*, & Luisi, B. (1994). The high-resolution crystal structure of a parallel-stranded guanine tetraplex. *Science* **265**, 520-524.

42. Aboul-ela, F., Murchie, A.I.H. & Lilley, D.M.J. (1992). NMR study of a parallel stranded tetraplex formation by d(TG$_4$T). *Nature* **360**, 280-282.

43. Wang, Y. & Patel, D.J. (1992). Guanine residues in d(T$_2$AG$_3$) and d(T$_2$G$_4$) form parallel-stranded potassium cation stabilized G-quadruplexes with anti glycosidic torsion angles in solution. *Biochemistry* **31**, 8112-8119.

44. Rich, A. (1993). DNA comes in many forms. *Gene* **135**, 99-109.

45. Saenger, W. (1984). *Principles of Nucleic Acid Structure.* Springer-Verlag, New York.

46. Tarasow, T.M. & Eaton, B.E. (1998). Dressed for success: realizing the catalytic potential of RNA. *Biopolymers* **48**, 29-37.

47. Fedoroff, O.Y., Salazar, M., Han, H., Chemeris, V., Kerwin, S.M. & Hurley, L.H. (1998). NMR-based model of a telomerase inhibiting compound bound to G-quadruplex DNA. *Biochemistry* **37**, 12367-12374.

48. Mergny, J.L. & Helene, C. (1998). G-quadruplex DNA: a target for drug design. *Nature Medicine* **4**, 1366-1367.

49. Lavallee, D.K. (1987). *The Chemistry and Biochemistry of N-Substituted Porphyrins.* VCH Publications, New York.

50. Smith, K.M. (1964). *Porphyrins and Metalloporphyrins.* Elsevier, Amsterdam.

51. Wang, Y., Hamasaki, K. & Rando, R.R. (1996). Specificity of aminoglycoside binding to RNA constructs derived from the 16S rRNA decoding region and the HIV-RRE activator region. *Biochemistry* **36**, 768-779.

52. Stryer, L. (1965). The interaction of a naphthalene dye with apomyoglobin and apohemoglobin. A fluorescent probe of non-polar binding site. *J. Mol. Biol.* **13**, 482-495.

53. Edsall, J.T. & Wyman, J. (1958). *Biophysical Chemistry.* Academic Press, New York.

54. Cheng, Y.C. & Prusoff, W.H. (1973). Relationship between the inhibition constant (*K*i) and the concentration of inhibitor which causes 50 per cent inhibition (I50) of enzymatic reaction. *Biochem. Pharmacol.* **22**, 3099-3108.

55. Cochran, A.G. & Schultz, P.G. (1990). Peroxidase activity of an antibody–heme complex. *J. Am. Chem. Soc.* **112**, 9414-9415.